JOURNAL OF THEORETICAL
AND APPLIED MECHANICS
64, 1, pp. 3–13, Warsaw 2026
https://doi.org/10.15632/jtam-pl/214041

INFLUENCE OF AIR VENT GEOMETRY IN BRAKE ROTORS ON THE PERFORMANCE OF A CAR BRAKING SYSTEM

Mateusz KITA*, Jarosław KACZMARCZYK, Sławomir DUDA

Department of Theoretical and Applied Mechanics, Silesian University of Technology, Gliwice, Poland
*corresponding author, *Mkita@polsl.pl*

The growing mass of modern vehicles increases kinetic energy and thermal stress on braking systems, elevating rotor temperatures and the risk of brake fade. In ventilated disc brakes, heat dissipation depends strongly on the geometry of internal vents. This study uses finite element method (FEM) simulations to examine the thermal behaviour of passenger-car ventilated rotors with different vent designs, including motorsport-inspired configurations, under high thermal loading. While previous studies have examined heat generation and dissipation in disc brakes, direct comparative FE analyses of vent geometries remain limited. The results demonstrate that vent shape significantly affects cooling performance during and following intense braking.

Keywords: finite element method; heat dissipation; brakes; friction coefficient.

1. Introduction

Brakes are essential vehicle components, enabling safe deceleration and speed control. Increasing vehicle mass and performance have driven continuous development of braking technology. Braking systems are commonly classified as stopping, holding, or retarding brakes, reflecting their functions. Early progress included the drum brake, introduced by Renault in 1902, and the disc brake concept proposed by Frederick William Lanchester in the same year; subsequent advances led to assistive technologies such as anti-lock braking systems (ABS), electronic brake-force distribution (EBD), and ultra-high-performance (UHP) tyres. The proliferation of electric vehicles has introduced regenerative braking; however, conventional friction-based systems remain critical for emergency braking, particularly in heavy vehicles (Nadig *et al.*, 2017; Cristescu & Ilie, 2023). Consequently, brake discs must combine high thermal capacity with efficient heat dissipation (Stefanelli *et al.*, 2024; Zhang & Zheng, 2024).

The primary objective of this study is to assess the influence of internal vent geometry on heat transfer and structural performance in ventilated rotors subjected to high-energy braking. Previous studies have developed theoretical models of disc temperature evolution (Talati & Jalalifar, 2008), applied FE methods to transient rotor heating (Gao & Lin, 2002), and demonstrated the predictive capability of FE-based thermal analyses (Belhocine & Bouchetara, 2013). However, systematic comparative investigations of internal vent geometries remain limited, thus motivating the present work.

Ministry of Science and Higher Education
Republic of Poland

This publication has been funded by the Polish Ministry of Science and Higher Education under the Excellent Science II programme "Support for scientific conferences".
The content of this article was presented during the 61st Symposium "Modelowanie w mechanice" (Modelling in Mechanics), Szczyrk, Poland, March 2–5, 2025.

2. Object of research

The analysed braking system is based on that of a Porsche Cayenne S Diesel (2013–2016). The front ventilated brake rotor has a diameter of 360 mm, which is typical for heavy sport utility vehicles (SUVs) and comparable to many electric vehicles in terms of thermal loading. The calliper is a six-piston design with pistons of 36 mm diameter each. In the numerical model, both pad-disc interfaces are accounted for through the normal force applied to the disc, calculated using Eq. (2.1), where A denotes the total effective area of all pistons acting on both sides of the rotor:

$$F = p \cdot A, \tag{2.1}$$

where F is the normal force acting on the brake pistons [N], p is the hydraulic pressure at the calliper inlet [Pa], A is the total effective area of all pistons acting on both sides of the rotor [m^2].

This axial force is transmitted to the brake disc, generating tangential friction force which depends on the coefficient of friction between the brake pad material and the disc:

$$F_f = F \cdot \mu, \tag{2.2}$$

where F_f is the friction force [N], μ is the coefficient of friction [–].

Since the brake pad contacts the disc at a finite radial distance from the disc axis, a braking torque is generated that enables the deceleration. This can be calculated as

$$M = F_f \cdot R', \tag{2.3}$$

where M is the braking torque [Nm], R' is the effective (nominal) braking radius [m].

Using the above formulas, the following input data are presented in Table 1 (Kalamegam *et al.*, 2025).

Table 1. Input parameters for braking torque estimation.

Total contact area of six brake pistons [mm^2]	6104.16
Hydraulic pressure at the brake calliper inlet [bar]	120
Normal force acting on brake pistons [N]	75 081
Coefficient of friction (assumed)	0.45
Average effective radius of friction force [mm]	150
Braking torque [Nm]	5000

2.1. Dynamometer tests of the friction coefficient

The experimental tests were conducted on a dynamometer stand designed to reproduce emergency braking conditions. The stand enables the simulation of braking torque, normal pressure, and disc rotational speed representative of real road conditions (Fig. 1). Pressure and torque were continuously monitored using high-precision sensors, while disc temperature was measured using thermocouples embedded in the disc body.

The hydraulic pressure measured at the outlet of the brake hose was approximately 12.6 MPa. This value corresponds to the actual pressure recorded on the vehicle under maximum braking conditions using a manometer. On the dynamometer stand, pressure was measured at an equivalent location corresponding to the brake hose connection; therefore, the same measurement approach was applied in both the experimental and numerical investigations.

Figure 2 presents the hydraulic pressure recorded during consecutive emergency braking events. The braking pressure remains within comparable limits; however, during the second emergency braking, the pressure increases to the maximum value achievable by the test stand,

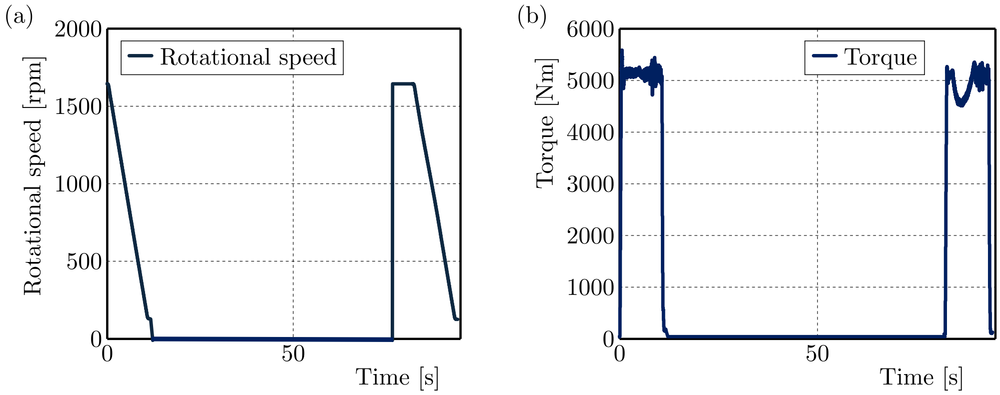

Fig. 1. (a) Rotational speed of the disc as a function of time; (b) braking torque as a function of time.

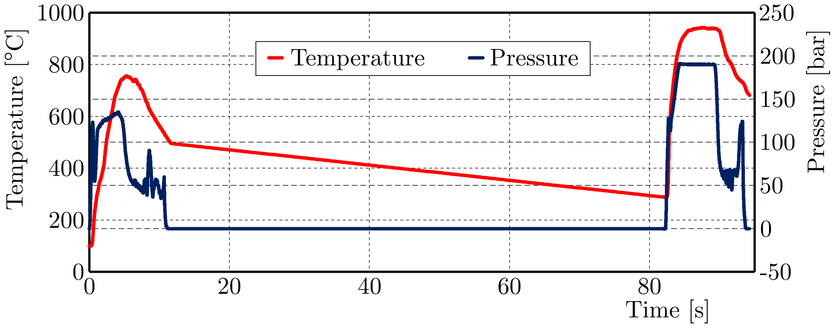

Fig. 2. Measured maximum temperature and pressure as functions of time during the test.

approximately 18 MPa. This increase can be attributed to phenomena such as partial degradation of the pad material, the onset of local fade and increased frictional instability. Although higher pressure is recorded, the effective contact stress at the pad–disc interface is reduced due to the distribution of forces over the piston area.

The friction coefficient was determined based on the measured braking torque, rotational speed, and hydraulic pressure using the following general relationship:

$$\mu(t) = \frac{M(t)}{p(t) \cdot A \cdot R'}, \tag{2.4}$$

where $\mu(t)$ is the friction coefficient, $p(t)$ is the hydraulic inlet pressure [Pa].

This equation reflects the actual test conditions, as both braking torque and hydraulic pressure were directly recorded during the experiments. The relationship between the torque and pressure signals was used to compute the temperature-dependent friction coefficient, providing a realistic $\mu(T)$ characteristic for simulation purposes.

The results indicate that the brake pad can maintain effective performance across a relatively wide temperature range. However, a noticeable drop in the friction coefficient occurs when temperatures exceed approximately 800 °C, as shown in (Fig. 2). During the second emergency braking event the dynamometer attempted to maintain constant braking torque and system inertia by automatically compensating for the falling friction coefficient through an increase in hydraulic pressure. Consequently, the pressure curve reached a maximum value of about 18 MPa, while the disc surface temperature exceeded 1000 °C. This phenomenon corresponds to brake fade, effectively concluding the simulation, since subsequent data no longer reflect realistic operating conditions.

The obtained data highlight the ineffectiveness of the tested braking system under high-temperature operating conditions. The primary issue lies in the insufficient cooling rate of the brake disc. As a result, the disc temperature before the second braking event remained at approximately 300 °C, in contrast to 100 °C at the beginning of the first braking.

2.2. Determination of the friction coefficient using experimental data

To improve the performance of the investigated braking system, the friction coefficient was determined as a function of temperature. Experimental data from Table 1, together with recorded time-dependent pressure and braking torque, were used to calculate the temperature-dependent friction coefficient employing the Coulomb–Moreau model. Subsequently, the LuGre friction model was implemented, utilising the friction coefficient obtained from the Coulomb-Moreau formulation. The LuGre friction coefficient was calculated according to Eq. (2.4), following Andrzejewski (2005):

$$\mu_L(t) = \mu_C(t) + (\mu_{\max} - \mu_C(t)) + \exp\left(\left(\frac{v_s}{v}\right)^2\right), \tag{2.5}$$

where $\mu_L(t)$ is the LuGre friction coefficient as a function of time [–], $\mu_C(t)$ is the Coulomb–Moreau friction coefficient as a function of time [–], $\mu_{\max}$ is the maximum calculated Coulomb–Moreau friction coefficient [–], v_s is the theoretical initial vehicle velocity, determined from the effective tyre radius at the road contact point [m/s], and v is the actual initial vehicle velocity [m/s]. The parameters used in the calculations are summarized in Table 2.

Table 2. Parameters utilised in the friction coefficient calculations.

Tyre size	295/35/R21
Nominal tyre radius [mm]	369.95
Tyre deflection during braking [mm]	1
Effective tyre radius at contact [mm]	359.95
Actual initial vehicle speed [km/h]	230
Theoretical vehicle speed v_s [km/h]	226.89

Using the parameters listed above, friction coefficient-temperature characteristics were obtained and are presented in Fig. 3.

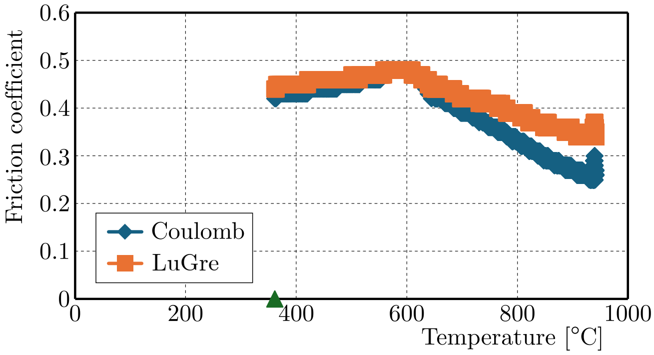

Fig. 3. Friction coefficient as a function of temperature calculated using Eqs. (2.4) and (2.5).

3. Numerical simulation of the original brake disc

The braking system was modelled using ANSYS Workbench. The geometry of the brake disc was developed and a finite element model was subsequently generated. The discretisation consisted of 441 440 tetrahedral elements and 739 304 nodes. The resulting geometry and finite element mesh are shown in Fig. 4.

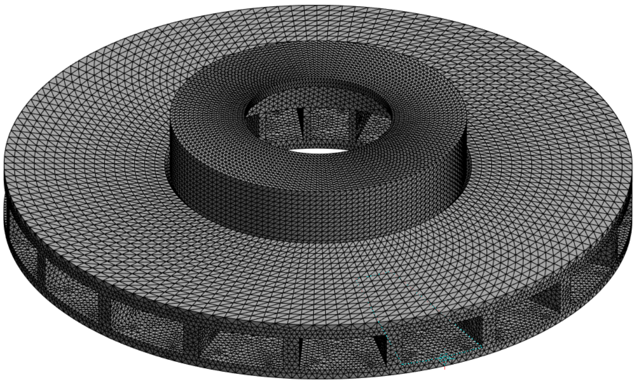

Fig. 4. Finite element mesh of the braking system.

Boundary conditions were applied to the model in the form of heat fluxes representing the thermal load generated by the brake pads during braking. These heat fluxes were imposed on the friction surfaces of the brake disc, where heat generation occurred. In addition, convective heat transfer was applied to the disc surfaces to account for cooling by the surrounding air.

Based on the experimental data, convective heat transfer was divided into two distinct mechanisms:

- localised convective heat transfer acting in regions characterised by intensified air turbulence, such as the ventilation channels and friction tracks of the disc,
- temperature-dependent surface convection applied exclusively to the inner and outer faces of the disc, with the heat transfer coefficient defined as a function of surface temperature.

The time-dependent convection coefficients used in the numerical simulations are summarised in Table 3.

Table 3. Convective heat transfer coefficients $[\mathrm{W/(m^2 \cdot {}^\circ C)}]$ as a function of time [s] for a temperature of $T = 22\,^\circ\mathrm{C}$.

Places where turbulent fluid flow is suspected		Places where laminar fluid flow is suspected	
Time [s]	Convection coefficient $[\mathrm{W/(m^2 \cdot {}^\circ C)}]$	Time [s]	Convection coefficient $[\mathrm{W/(m^2 \cdot {}^\circ C)}]$
0	90	0	70
1	90	1	70
2	92	2	72.5
3	94	3	75
4	97	4	77.5
5	106	5	80
6	120	6	87
6.67	110	6.67	88
7	95	7	85
20	76	20	76
40	72	40	72
83	70	83	70

Subsequently, the remaining material properties were introduced into the model, including temperature-dependent Young's modulus, Poisson's ratio, and specific heat capacity (Agrawal *et al.*, 2024). These properties are essential for accurately capturing the coupled thermal and structural response of the brake disc under elevated-temperature conditions (De Freitas *et al.*, 2023; Kalamegam *et al.*, 2025). The applied material data are presented in Fig. 5 and Table 4.

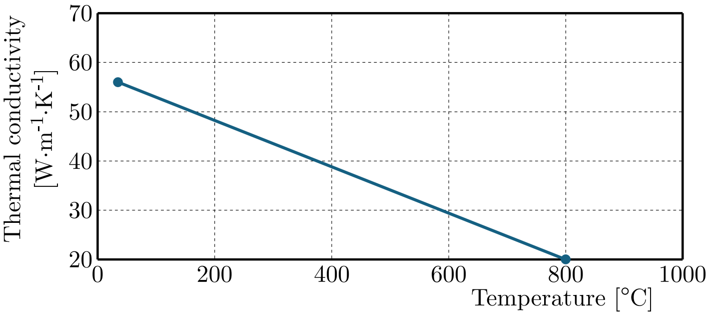

Fig. 5. Thermal conductivity as a function of temperature (Bentz & Prasad, 2007).

Table 4. Specific heat as a function of temperature (Kim *et al.*, 2012).

	Temperature [°C]	Specific heat $[\mathrm{J} \cdot \mathrm{kg}^{-1} \cdot \mathrm{K}^{-1}]$
1	0	447
2	100	470
3	200	505
4	300	555
5	400	610
6	500	670
7	600	740
8	700	850

To determine the heat flux applied to the brake disc surface during braking, the following procedure was adopted. The total kinetic energy of the vehicle was first calculated as

$$KE = \frac{m\Delta v^2}{2} = \frac{2700 \cdot 63.5^2}{2} = 5\,645\,150\,[\mathrm{J}], \tag{3.1}$$

where KE is the total kinetic energy of the moving vehicle [J], m is the vehicle mass with a full fuel tank and full load [kg], and v is the vehicle velocity [m/s].

The calculations were based on experimental data and standard assumptions. It was assumed that 3 % of the generated heat was absorbed by the brake pad material, while 5 % of the total kinetic energy was dissipated due to aerodynamic drag. After accounting for these losses, 80 % of the remaining energy was assigned to the front axle, in accordance with the ECE R90 regulation. This approach ensures that the energy distribution corresponds to standardised vehicle homologation conditions. Although the exact energy distribution may vary for a specific vehicle, the use of ECE R90 assumptions ensures comparability and reproducibility of the results. Consequently, the portion of kinetic energy dissipated by a single front brake disc was calculated as

$$E = KE \cdot \gamma \cdot k = 5\,645\,150 \cdot (1 - 0.03) \cdot (1 - 0.05) \cdot 0.8 \cdot 0.5 = 2\,080\,802\,[\mathrm{J}], \tag{3.2}$$

where E is the kinetic energy dissipated by one brake disc [J], k is the coefficient accounting for additional energy losses (e.g., aerodynamic drag), and γ is the fraction of energy assigned to the disc under consideration.

The average braking power was then obtained by dividing the dissipated energy by the braking time:

$$P_b = \frac{E}{t} = \frac{2\,080\,802}{5.85} = 356\,117.8\,[\mathrm{W}], \tag{3.3}$$

where t is the braking time [s].

The heat flux q [W/mm^2] applied to the disc friction surfaces was calculated by dividing the braking power by the effective friction surface area A_p [m^2] of the two brake pads in contact with the disc:

$$q = \frac{P_b}{A_p} = \frac{356\,117.8}{0.19} = 1\,874\,304\,[\mathrm{W/m^2}] \sim 2\,[\mathrm{W/mm^2}], \tag{3.4}$$

where A_p is the effective contact area of the pads on both sides of the rotor [m^2], q is the heat flux [W/mm^2].

Finally, the stopping distance s [m] was calculated as

$$s = \frac{v^2}{2 \cdot a} = \frac{63.5^2}{2 \cdot 10.87} = 185.51\,[\mathrm{m}], \tag{3.5}$$

where a is the vehicle deceleration achieved with OE Yokohama Advan Sport V105 tyres [m/s^2].

Based on these results, the input parameters listed in Table 5 were defined for the transient thermal simulation conducted in ANSYS.

Table 5. Input parameters used in the transient thermal and structural simulations conducted in ANSYS.

Number of steps	12
Time step	Program controlled
Heat flux [W/m^2]	2 000 000
Number of nodes	739 304
Number of elements	481 440
Initial temperature [°C]	100

After configuring the aforementioned parameters (López-Flores *et al.*, 2024; Piasecka-Belkhayat & Kowalski, 2018; Najmi *et al.*, 2021; Sainath *et al.*, 2021), the numerical simulation was performed. The finite element analysis yielded the temperature distribution at the instant of maximum thermal loading, as shown in Fig. 6.

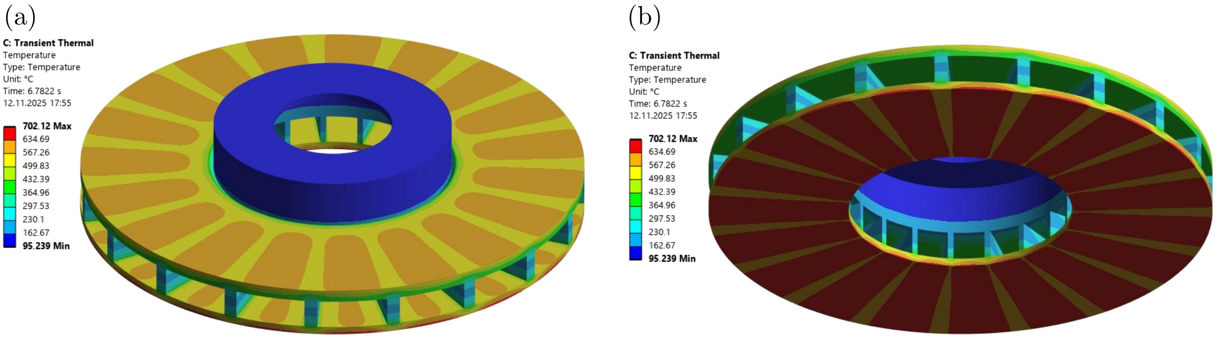

Fig. 6. Temperature distribution in the brake disc: (a) top view; (b) bottom view.

Subsequently, a transient structural analysis was conducted using the temperature field obtained from the thermal simulation as input. This analysis was performed to evaluate the stress and deformation response of the brake disc under thermo-mechanical loading conditions representative of emergency braking. The resulting stress and deformation fields are presented in Fig. 7.

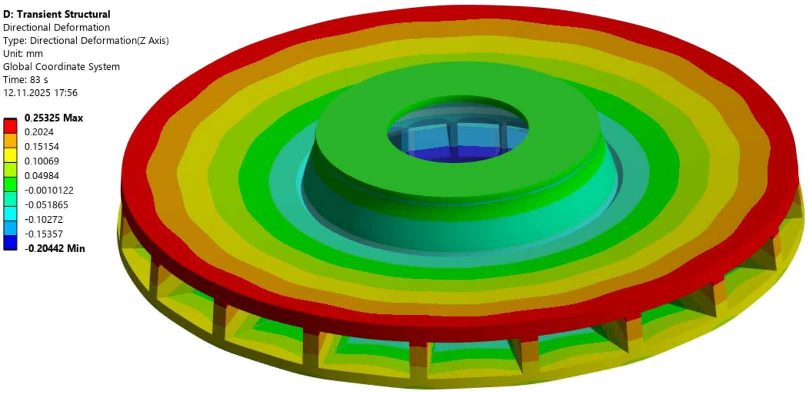

Fig. 7. Contour plots of deformation along the z-axis obtained from the transient structural analysis.

4. Upgrade of the brake disc ventilation

The original brake disc model was upgraded, based on design principles observed in ceramic brake discs commonly used in high-performance applications, including Formula 1 vehicles (Dinesh Kumar & Darius Gnanaraj, 2023). The use of small 13-inch rims constrained the maximum allowable rotor diameter. Consequently, a compact disc rotor with an increased number of smaller ventilation channels was developed. The primary design objectives were to accelerate the cooling process during dynamic driving and to minimise thermally induced deformation of the disc (Al Riyami *et al.*, 2023; Skonieczna & Ptaszny, 2017).

Figure 8 presents the geometry of the upgraded brake disc, together with the corresponding temperature and deformation distributions. To reduce computational cost, only a four-degree sector of the full disc geometry was modelled in the numerical simulations.

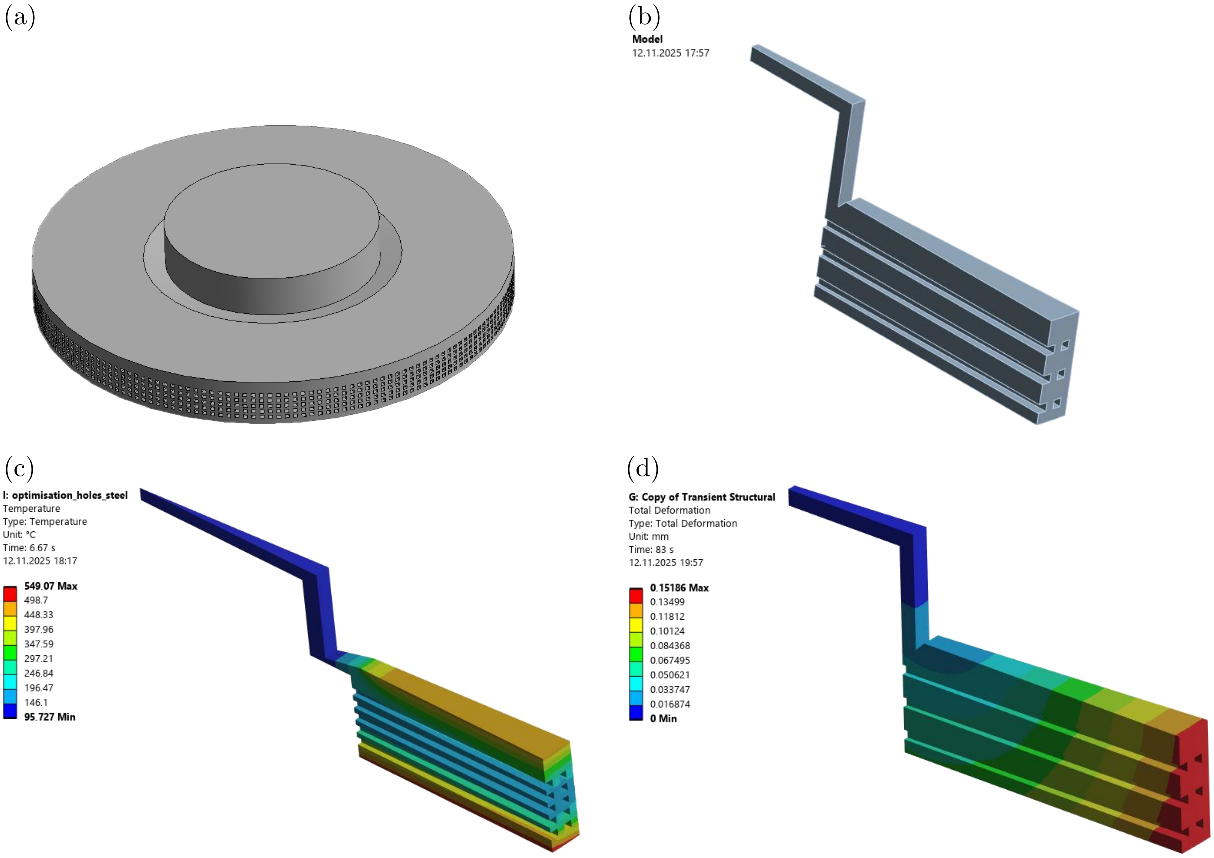

Fig. 8. Braking system: (a) upgraded disc rotor; (b) three-degree part of the rotor; (c) contour plots of temperature during braking; (d) contour plots of deformation during braking.

5. Comparison of temperature variation between the original and upgraded discs

Figure 9 illustrates the temperature distributions obtained for both the original and upgraded brake discs designs under high-load braking conditions. Both variants reached their maximum temperature after approximately 4 s of braking. However, the upgraded disc exhibited a significantly lower peak temperature and a faster cooling rate compared to the original design. This improvement is attributed to enhanced airflow through the redesigned internal ventilation channels, which increased the effective convective heat transfer surface area of the rotor. As a result, the upgraded disc experienced lower average temperatures leading to reduced thermal stress and deformation.

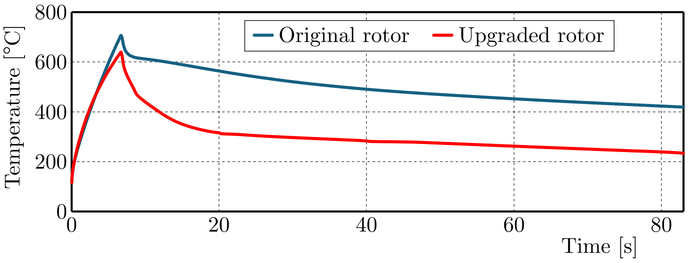

Fig. 9. Relationship between maximum temperature and time for the original rotor, and the upgraded rotor.

Subsequently, the size and number of ventilation holes in the brake disc were optimised to minimise both temperature and stress, while simultaneously reducing the mass of the brake disc (Dinesh Kumar & Darius Gnanaraj, 2023). Disc thickness was also included in the optimisation process. To reduce computational effort, the thermal optimisation objective was restricted to minimising the maximum temperature at the end of the disc cooling simulation. This approach was justified by earlier results, which had already demonstrated the improved thermal performance of the modified disc design.

The optimisation was conducted using the multi-objective genetic algorithm (MOGA) implemented in the ANSYS software. The following parameters were applied:

- an initial population of 42 samples,
- 42 samples per iteration,
- identification of the 3 best candidate solutions,
- a maximum number of 7 iterations.

This methodology enabled an efficient exploration of the design space while balancing competing objectives, including thermal performance, structural integrity, and mass reduction.

Three candidate design configurations were identified (Table 6).

Table 6. Three best candidate configurations found during optimisation.

	Parameter	Candidate point 1	Candidate point 2	Candidate point 3
1	P1-Holes_H [mm]	3.3	3.2246	2.7389
2	P2-Holes_Number	180	179	166
3	P3-Holes_H2 [mm]	3.3093	2.7261	3.0257
4	P4-Holes_Distance-V [mm]	9.5198	9.3847	9.4606
5	P5-Thick_Rotor [mm]	38.168	41.34	40.876
6	P6-Temperature_Maximum [°C]	184.94	260.91	260.45
7	P7-Solid Mass [kg]	0.17938	0.21588	0.2164
8	P8-Equivalent Stress Maximum [MPa]	446.13	526.91	525.77
9	P9-Total Deformation Maximum [mm]	0.24265	0.34941	0.35174

Among these, candidate one exhibited the lowest maximum temperature and stress levels among all analysed configurations. Its parameters were as follows: hole height of 3.3 mm, axial spacing of 3.3 mm, disc thickness of 38.1 mm, distance from the first hole of 9.5 mm, total number of holes of 180, and rotor mass of 15.5 kg.

At the time of the initial study, the mass of the upgraded disc was slightly higher than that of the original model due to the thicker central web required to accommodate the revised duct geometry. Further design development led to the introduction of a honeycomb-style ventilation system, which significantly improved both thermal and structural performance. The honeycomb pattern provided an optimal balance between rigidity and cooling surface area, resulting in a measurable reduction in rotor mass while maintaining lower peak operating temperatures compared to the original design.

6. Conclusions

This study presented a coupled thermal and structural analysis of a ventilated brake disc from the Porsche Cayenne S Diesel braking system. Dynamometer testing demonstrated that the original disc design provided insufficient cooling during repeated emergency braking events, whereas the modified vented design, inspired by motorsport ceramic brake concepts, achieved lower peak temperatures and faster cooling rates, thereby reducing the risk of brake fade.

The LuGre friction model, calibrated using dynamometer data, successfully captured the temperature-dependent behaviour of the pad–disc interface and improved the accuracy of numerical simulations. Optimisation using genetic algorithms identified an optimal disc configuration that effectively balanced thermal efficiency, structural durability, and mass reduction.

Overall, the results emphasise the importance of integrated thermal–structural analysis and optimisation in contemporary brake system design. The proposed methodology offers practical guidance for improving braking systems in heavy SUVs and electric vehicles, where extreme thermal loads are increasingly common.

References

1. Agrawal, V.K., Patil, L.N., Chavan, K.V., & Nimbalkar, U.D. (2024). A computational analysis of heat transfer in solid and vented disc brakes: CFD simulation and thermal performance assessment. *Multiscale and Multidisciplinary Modeling, Experiments and Design*, *7*(5), 4735–4749. https://doi.org/10.1007/s41939-024-00400-y
2. Al Riyami, S.S., Chala, G.T., Bernard, A., & Al Maawali, K. (2023). A case study on thermal analysis of the disc brake used for heavy-duty cars. *PLATFORM – A Journal of Engineering*, *7*(2), 21–32. https://files01.core.ac.uk/download/579834390.pdf
3. Andrzejewski, R. (2005). Models of drive wheel traction. Friction models (in Polish). *Archiwum Motoryzacji*, *1*, 59–76.
4. Belhocine, A., & Bouchetara, M. (2013). Investigation of temperature and thermal stress in ventilated disc brake based on 3D thermomechanical coupling model. *Ain Shams Engineering Journal*, *4*(3), 475–483. https://doi.org/10.1016/j.asej.2012.08.005
5. Bellini, C., Di Cocco, V., Iacoviello, D., & Iacoviello, F. (2024). Temperature influence on brake pad friction coefficient modelisation. *Materials*, *17*(1), Article 189. https://doi.org/10.3390/ma17010189
6. Bentz, D.P., & Prasad, K.R. (2007). *Thermal performance of fire resistive materials. I. Characterization with respect to thermal performance models*. National Institute of Standards and Technology. https://www.researchgate.net/publication/241211063
7. Cristescu, A.C., & Ilie, F. (2023). Influence of travel speed, time, and distance of braking on the efficiency of a car's braking system. *Preprints*, https://doi.org/10.20944/preprints202310.1358.v1
8. De Freitas, T.V.A., Rodrigues, R.N., Costa, C.A.S., Bezerra, R.A., Gonçalves, V.V., Maciel, M.H.C., & Queiroz, D.M. (2023). Influence of design parameters in the brake squeal in electric cars. *Revista Brasileira de Física Tecnológica Aplicada*, *10*(2), 39–53. https://revistas.utfpr.edu.br/rbfta/article/viewFile/17352/9940

9. Dinesh Kumar, P.K., & Darius Gnanaraj, S. (2023). Aluminium-silicon based metal matrix composites for brake rotor applications: a review. *Engineering Research Express*, *5*(2), Article 022002. https://doi.org/10.1088/2631-8695/accdb6
10. Gao, C.H., & Lin, X.Z. (2002). Transient temperature field analysis of a brake in a non-axisymmetric three-dimensional model. *Journal of Materials Processing Technology*, *129*(1–3), 513–517. https://doi.org/10.1016/S0924-0136(02)00622-2
11. Kalamegam, P., Chong, P.L., Faraji, F., Moey, L.K., Manan, M.S.A., & Roy, S. (2025). A comparative study of thermo-mechanical performance of brake rotor discs using finite element analysis. *International Journal on Interactive Design and Manufacturing*, 19(7), 5383–5395. https://doi.org/10.1007/s12008-024-02139-9
12. Kim, B.G., Rempe, J.L., Knudson, D.L., Condie, K.G., & Sencer, B.H. (2012). In-situ creep testing capability for the advanced test reactor. *Nuclear Technology*, *179*(3), 417–428. https://doi.org/10.13182/NT12-A14173
13. López-Flores, J.-G., Cordero-Guridi, J. de J., Ovando-Cuevas, E.R., & Yescas-Ávila, E.A. (2024). Thermal-structural numerical analysis of the brake and disc system of a Formula SAE 2024 type vehicle. *Journal-Mathematical and Quantitative Methods*, *8*(14), Article e30814113. https://doi.org/10.35429/JMQM.2024.8.14.3.13
14. Nadig, D.S., Shivakumar, P., Anoop, S., Chinmay, K., Divine, P.V., & Harsha, H.P. (2017). Effects of cryogenic treatment on the wear properties of brake discs. *IOP Conference Series: Materials Science and Engineering*, *171*, Article 012152. https://doi.org/10.1088/1757-899X/171/1/012152
15. Najmi, H., Kumar, N., Himanshu, Singh, A., Singh, R., & Kumar, S. (2021). Thermal analysis of brake disc of an automobile. *IOP Conference Series: Materials Science and Engineering*, *1116*, Article 012146. https://doi.org/10.1088/1757-899X/1116/1/012146
16. Piasecka-Belkhayat, A., & Kowalski, P. (2018). Numerical modeling of heat transfer in biological tissue domain using the fuzzy finite difference method. In R. Owen, R. de Borst, J. Reese, & C. Pearce (Eds.), P*roceedings of the 6th. European Conference on Computational Mechanics (Solids, Structures and Coupled Problems): ECCM 6; 7th. European Conference on Computational Fluid Dynamics: ECFD 7* (pp. 1475–1484). International Center for Numerical Methods in Engineering (CIMNE). http://congress.cimne.com/eccm_ecfd2018/frontal/docs/Ebook-Glasgow-2018-ECCM-VI-ECFD-VII.pdf
17. Sainath, A., Dehadray, P.M., Bharath, P., & Rao, L.B. (2021). The thermal and stress analysis of disc brake. *IOP Conference Series: Materials Science and Engineering*, *1128*, Article 012015. https://doi.org/10.1088/1757-899X/1128/1/012015
18. Skonieczna, D., & Ptaszny, J. (2017). Strengh analysis of the stabilizer bar link (in Polish). In G. Dziatkiewicz, J. Ptaszny, & M. Dziewoński (Eds.), *Metody komputerowe – 2017: Studencka konferencja naukowa, Gliwice, maj 2017* (pp. 65–68). Silesian University of Technology.
19. Stefanelli, A., Aprea, M., Carbone, F., Romagnuolo, F., Caresia, P., & Suero, R. (2024). Integrated thermomechanical analysis of tires and brakes for vehicle dynamics and safety. *Vehicles*, *6*(3), 1637–1647. https://doi.org/10.3390/vehicles6030077
20. Szymczak, T., Kowalewski, Z.L., & Brodecki, A. (2025). Durability tests for the automotive industry. *Journal of Theoretical and Applied Mechanics*, *63*(3), 461–469. https://doi.org/10.15632/jtam-pl/200388
21. Talati, F., & Jalalifar, S. (2009). Analysis of heat conduction in a disk brake system. *Heat and Mass Transfer*, *45*(8), 1047–1059. https://doi.org/10.1007/s00231-009-0476-y
22. Zhang, Z., & Zheng, S. (2024). Characterization of temperature rise of carbon ceramic brake disc. *Journal of Physics: Conference Series*, *2827*, Article 012011. https://doi.org/10.1088/1742-6596/2827/1/012011

Manuscript received June 24, 2025; accepted for publication November 6, 2025;